ARTICLE OPEN

Check for updates

Theory of superconductivity in doped quantum paraelectrics

Yue Yu[1,2], Harold Y. Hwang[1,2], S. Raghu[1,2]✉ and Suk Bum Chung[3,4]✉

Recent experiments on Nb-doped $SrTiO_3$ have shown that the superconducting energy gap to the transition temperature ratio maintains the Bardeen–Cooper–Schrieffer (BCS) value throughout its superconducting dome. Motivated by these and related studies, we show that the Cooper pairing mediated by a single soft transverse-optical phonon is the most natural mechanism for such a superconducting dome given experimental constraints, and present the microscopic theory for this pairing mechanism. Furthermore, we show that this mechanism is consistent with the T^2 resistivity in the normal state. Lastly, we discuss what physical insights $SrTiO_3$ provides for superconductivity in other quantum paraelectrics such as $KTaO_3$.

npj Quantum Materials (2022)7:63 ; https://doi.org/10.1038/s41535-022-00466-2

INTRODUCTION

The observation of superconductivity in "quantum paraelectrics"—materials with low temperature incipient ferroelectricity—has raised several fundamental questions on the pairing mechanism in such systems. Examples of quantum paraelectrics include strontium titanate ($SrTiO_3$)[1–6] as well as potassium tantalate ($KTaO_3$)[7–10] and lead telluride (PbTe)[11]. A central question involves the hierarchy of the relevant fluctuations and their consequences for superconductivity. For instance, if pairing is mediated mainly by soft critical ferroelectric fluctuations, the associated superconducting dome would be confined to low electron densities, as ferroelectricity itself is sharply defined only in an insulating phase (A "ferroelectric metal" is essentially characterized by either broken inversion, i.e. non-centrosymmetric, or spatial reflection symmetries[12]; dipole moments while permitted by symmetry, are strongly screened by the conduction electrons.). The fact that superconductivity, at least in niobium-doped strontium titanate, is observed only over a range in the dilute limit (~0.05% to ~0.5%)[3,4,6] gives support to the notion of pairing mediated by ferroelectric fluctuations[13].

The restriction of pairing to dilute carrier concentrations, however, presents several puzzling issues. First, the resulting small density of states in a 3*d* electron system would suggest a correspondingly small superconducting pairing strength. Second, the soft mode associated with ferroelectricity is the transverse-optical (TO) phonon, which couples less strongly to the electrons than the longitudinal optical (LO) phonons. Moreover, symmetry considerations lead to the conclusion that in the absence of orbital- or spin-dependent processes, electrons can only scatter off of pairs of TO phonons[14–16]. The resulting reduction in phase space would naturally result in reduction of the superconducting transition temperature T_c. Finally, given the dilute electron concentrations, there is the possibility that the Fermi energy may be smaller than the phonon frequency itself, resulting in an inverted "anti-adiabatic" pairing regime. Whether superconducting domes can arise in quantum paraelectrics despite these circumstances remains actively debated[17–21]. Moreover, the observation of superconductivity at interfaces of quantum paraelectrics[7–10,22,23] further motivates the study of superconductivity in these systems, raising the question of the role of spatial dimensionality on all these issues.

In this Letter, we construct a self-consistent pairing scenario for quantum paraelectrics, and illustrate it in the case of $SrTiO_3$, where recent experiments have placed significant constraints on theory. These experiments have reported a textbook BCS gap to T_c ratio[4–6]; any theory of pairing in this system must satisfy this constraint. In light of these experiments, we discuss constraints on pairing that arises from either the anti-adiabatic or the more conventional adiabatic pairing mechanisms. We construct a scenario in which pairing is mediated by TO phonons. We also present a mechanism by which electrons may couple to single TO phonons, resolving the issues of limited phase space alluded to above. We then discuss the relevance of these findings to other quantum paraelectrics, including interfacial systems.

RESULTS

Experimental considerations

Two distinct pairing scenarios have been proposed to explain superconductivity in the dilute limit of bulk $SrTiO_3$: a conventional one in which the phonon frequency remains smaller than the Fermi energy E_F[24–27], and an anti-adiabatic mechanism in which the hierarchy of energy scales are inverted[28–35]. In recent experiments[4,6], various phonon frequencies were probed, in addition to the superconducting gap. Various experiments also show that (1) the lowest TO (TO1) phonon frequency increases with doping but remains below the Fermi energy across the superconducting dome[6,36,37], (2) the LO phonon frequencies remain unchanged with doping and are either comparable to or greater than E_F across the dome[38], and (3) the superconducting gap to T_c ratio is close to the BCS value[4–6].

It follows from the first observation that any pairing mechanism involving the TO1 phonons can remain conventional and adiabatic whereas LO pairing mechanisms would be in the anti-adiabatic regime in $SrTiO_3$. We first briefly describe why the anti-adiabatic scenarios are unlikely in $SrTiO_3$ and we then consider the adiabatic pairing scenario mediated by TO phonons.

Based on the tunneling measurements[4–6], any anti-adiabatic pairing scenario that remains viable across the superconducting dome must necessarily only involve the highest LO phonon mode (LO4). Furthermore, the constraint imposed by the BCS gap to T_c ratio requires the effective attraction mediated by the LO phonon

[1]Stanford Institute for Materials and Energy Sciences, SLAC National Accelerator Laboratory, Menlo Park, CA 94025, USA. [2]Geballe Laboratory for Advanced Materials, Stanford University, Stanford, CA 94305, USA. [3]Department of Physics and Natural Science Research Institute, University of Seoul, Seoul 02504, Republic of Korea. [4]School of Physics, Korea Institute for Advanced Study, Seoul 02455, Republic of Korea. ✉email: sraghu@stanford.edu; sbchung0@uos.ac.kr

to be weak, which can occur in the anti-adiabatic regime only if the LO4 phonon frequency were significantly higher than the Fermi energy. Further restrictions from the tunneling data come from the fact that the LO frequency remains essentially unchanged with doping. Since the BCS coupling is proportional both to the density of states and the square of electron-phonon coupling, a crucial ingredient needed for T_c to decrease beyond optimal doping is the reduction of the electron-phonon coupling strength with the dopant concentration n faster than $n^{-1/3}$, in order to overcome the growth of the BCS coupling with increasing density of states. It therefore seems unlikely, based in part on the tunneling measurements, that pairing in $SrTi_{1-x}Nb_xO_3$ is mediated by an anti-adiabatic LO4 phonon.

We are thus led naturally to consider an adiabatic pairing mechanism across the dome of $SrTi_{1-x}Nb_xO_3$. The only phonon mode that remains in the adiabatic regime across the dome is the TO1 mode, the softening of which leads to ferroelectricity. Furthermore, a conventional BCS framework based on the Migdal approximation should suffice to account for the BCS gap to T_c ratio within this scenario (The lower density dome that is observed in oxygen-reduced samples[3] is outside the scope of the present paper as such samples have been resistant to the pairing gap measurement through the planar tunneling spectroscopy.).

Additionally, the superconducting dome from TO1 phonon exchange can be simply understood as follows. Prior experiments[36,37] indicate that the TO1 phonon frequency increases with carrier concentration as $\omega_T^2 = K_0 + nK_1$ with the approximate values of $K_0 \approx 1\,\mathrm{meV}^2$ and $K_1 \approx 1.8 \times 10^{-19}\,\mathrm{meV}^2\,\mathrm{cm}^3 > 0$[15]. Hence the BCS eigenvalue for the adiabatic pairing mediated solely by a single TO1 phonon is parametrically:

$$\lambda_{\mathrm{BCS}} \propto \frac{N_F}{\omega_T^2} \sim \frac{n^{1/3}}{K_0 + K_1 n}; \tag{1}$$

the overdoped attenuation of T_c naturally comes from the fact that the TO1 phonon hardens "faster" with Nb concentration than the increase in the density of states. Thus, in the adiabatic pairing scenario based on TO1 phonon exchange, the low density edge of the dome is dictated by the vanishing of the density of states whereas the high density edge is dictated by the hardening of the phonon frequency (in conjunction with the Coulomb pseudopotential μ^*).

The only caveat in the hypothesis above is that it assumes a conventional coupling of the electrons to a single TO phonon. Symmetry considerations however, require that if the initial and final electron states in a phonon exchange process have the same symmetry with respect to reflection about the plane normal to which the TO mode displacement occurs, the process must involve a pair of TO phonons[39] (for discussion on superconductivity arising from such electron-phonon coupling, see ref. [16]). As we discuss below, the way around this constraint is to include multiple orbitals; a single TO phonon can scatter an electron from an orbital that is even under such a reflection to one that is odd, and vice-versa[40]. As we show, such processes can naturally account for a superconducting dome in this system.

Pairing from TO phonon scattering

The qualitative effect of the electronic coupling to the single TO1 phonon can be most simply obtained from a microscopic model for the $SrTiO_3$ electronic band structure that incorporates the titanium (Ti) $3d t_{2g}$ orbitals while assuming the simple cubic lattice structure. The low-energy band structure can be described well by a minimal tight-binding model whose k-space representation can be written as refs. [15,41–43]:

$$H_0 = \sum_{\mathbf{k},\alpha,s} (\epsilon_\alpha - \mu) c^\dagger_{\mathbf{k},\alpha,s} c_{\mathbf{k},\alpha,s} - \frac{\xi}{2} \sum_{\mathbf{k},\alpha,\beta,s,s'} \ell_{\alpha\beta} \cdot \boldsymbol{\sigma}_{s,s'} c^\dagger_{\mathbf{k},\alpha,s} c_{\mathbf{k},\beta,s'}, \tag{2}$$

where $\alpha, \beta = X, Y, Z$ refer, respectively, to the Ti d_{yz}, d_{xz}, d_{xy} orbitals, s, s' the spin indices, $\xi = 19.3$ meV from the Ti atomic spin-orbit coupling with the totally antisymmetric tensor $\ell^\alpha_{\beta\gamma} \equiv -i\varepsilon_{\alpha\beta\gamma}$ representing the effective $L = 1$ orbital angular momentum of the TI t_{2g} orbitals, and:

$$\epsilon_\alpha = \epsilon_0 + 4t_1 \sum_{\beta \neq \alpha} \sin^2 \frac{k_\beta}{2} + 4t_2 \sin^2 \frac{k_\alpha}{2}, \tag{3}$$

is the intra-orbital hopping (with $\epsilon_0 = 12.2$ meV) whose $t_1 > t_2$ anisotropy (0.615 and 0.035 eV, respectively) can be attributed to the quantum mechanical effect of the Ti t_{2g} orbital symmetry[15,42].

The form of the electronic coupling to the TO1 phonons is determined by the interplay between the t_{2g} orbital symmetry and the crystalline structure. As shown in Fig. 1, the tunneling between different t_{2g} orbitals between nearest neighbors is forbidden by inversion symmetry in a static lattice, but the TO1 mode displacements break inversion symmetry and thereby induce odd-parity inter-orbital tunneling. Given its odd-parity, this tunneling at the long-wavelength limit can be described by the following electron-phonon interaction[44,45]:

$$H_{e-p} = g \sum_{\mathbf{k},\mathbf{q}} \sum_{i,\alpha,\beta,s} \boldsymbol{\phi}_{\mathbf{q}} \cdot [\ell_{\alpha\beta} \times (\mathbf{k} + \mathbf{q}/2)] c^\dagger_{\mathbf{k}+\mathbf{q},\alpha,s} c_{\mathbf{k},\beta,s} \tag{4}$$

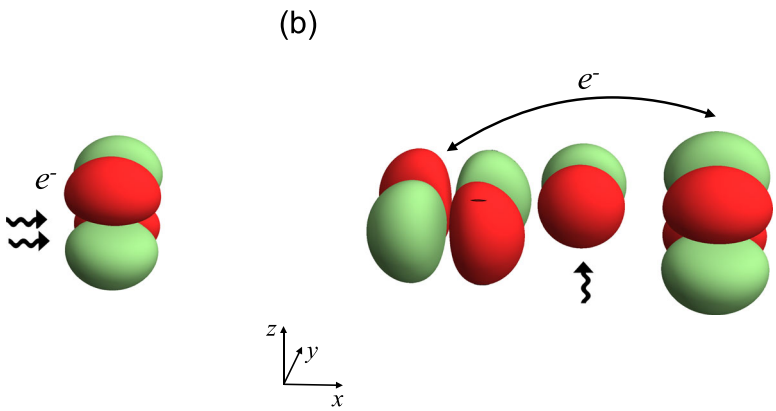

Fig. 1 Electron coupling to TO1 phonon. Two types of symmetry allowed couplings between t_{2g} electrons and the TO phonons. In a two phonon process (**a**), a pair of TO phonons, each denoted by a wavy line oriented along the displacement axis, couples to the electron density. **b** Single-phonon processes can occur provided the tunneling occur between two distinct t_{2g} orbitals on the nearest neighbors. Along the crystalline x axis, a TO displacement along the z-direction couples the d_{xy} and d_{yz} orbitals. The wavy line denotes the TO phonon displacement axis.

where $\boldsymbol{\phi}$ is the TO1 mode displacement vector. The simplest justification for this coupling is to consider a uniform $\boldsymbol{\phi}\|\hat{\mathbf{z}}$, which would displace the Ti atom from the center of TiO_6 octahedron along the z-direction by a constant amount; this will turn on the nearest-neighbor hopping between the d_{xy} and d_{yz} (d_{xz}) in the x(y)-direction through the O p_y (p_x) orbital. The following two aspects of this electron-phonon coupling makes it viable as the pairing glue for superconductivity.

First, the electron-phonon coupling of Eq. (4) is distinct from acoustic phonons coupling derivatively to the fermions. As long as there is a non-zero fermion density, the typical fermion momentum $|\boldsymbol{k}| \sim k_F$ is finite, and the electron-phonon coupling in Eq. (4) survives even in the $q \to 0$ limit. In the interest of simplicity, we consider the case where gk_F is independent of density; what this implies will be discussed upon obtaining the effective BCS interaction.

Second, the electron-phonon coupling of Eq. (4) can induce an intra-band pairing interaction due to the presence of atomic spin-orbit coupling in Eq. (2)[46–48]. This is not limited to the three C_3 rotational axes of the cubic lattice, where the eigenstates of the H_0 of Eq. (2) are the effective $j = 1/2$ and $j = 3/2$ states (The projections of $\boldsymbol{\phi} \cdot (\boldsymbol{\ell} \times \mathbf{k})$ to the $j = 1/2$ and the $j = 3/2$ subspaces are $\frac{4}{3}\boldsymbol{\phi} \cdot (\mathbf{j} \times \mathbf{k})$ and $-\frac{2}{3}\boldsymbol{\phi} \cdot (\mathbf{j} \times \mathbf{k})$, respectively[49,50]). Even away from this band degeneracy, the intra-band Rashba coupling of the TO1 phonon[27,51,52] can be obtained by treating the sum of Eq. (4) and the atomic spin-orbit coupling of Eq. (2) as perturbations[48,53].

We now derive the dimensionless effective BCS pairing interaction from this electron-phonon coupling using the Dyson's equation in the Nambu space where the electron self-energy arises entirely from the Cooper pairing. For this Dyson's equation:

$$\Sigma(\mathbf{k}, i\nu_m) = 2\tfrac{k_B T}{\hbar} \sum_{\mathbf{k}', i,j} \chi_{ij}(\mathbf{k} - \mathbf{k}') \times F_j(\mathbf{k}, \mathbf{k}' - \mathbf{k}) \mathcal{G}(\mathbf{k}', i\nu_m) F_i(\mathbf{k}, \mathbf{k}' - \mathbf{k}), \tag{5}$$

where $\nu_m \equiv (2m+1)\pi k_B T/\hbar$ (with $m \in \mathbb{Z}$) is the fermionic Matsubara frequency, $\mathcal{G}$ the electronic Green's function and:

$$F_i(\mathbf{k}, \mathbf{k}' - \mathbf{k}) \equiv g[\ell \times (\mathbf{k} + \mathbf{k}')]_i/4 \tag{6}$$

is the electron-phonon interaction vertex from Eq. (4), with $g \propto n^{-1/3}$ to maintain an effective electron-phonon coupling strength independent of the carrier density n. We take advantage of the adiabaticity of the TO1 phonon to ignore the boson dynamics[27] and take the static TO1 propagator:

$$\chi^{ij}(\mathbf{q}) = \langle \phi^i_{-\mathbf{q}} \phi^j_{\mathbf{q}} \rangle = \frac{\hbar}{M_T} \frac{\delta_{ij} - \hat{q}_i \hat{q}_j}{\omega_T^2 + c_T^2 q^2}, \tag{7}$$

where M_T is the TO1 phonon effective mass. Given that the self-energy for this Dyson's equation is given as the linear combination of the pairing gap, we need to consider the form of pairing gap that would be favored by the electron-phonon coupling of Eq. (4). With regards to the Cooper pair spin states, we note that any electron-phonon coupling, even with odd-parity, favors spin-singlet pairing[46,47,52,54]. Therefore our pairing gap should be intra-band, even-parity, pseudospin-singlet (frequency-independence being already assumed by Eq. (5)), giving us:

$$\Sigma(\mathbf{k}) = \tau^x u(\mathbf{k}) \Delta(\mathbf{k}) (i\sigma^y \delta[\alpha_{\mathbf{k}}]) u^T(-\mathbf{k}), \tag{8}$$

written in orbital basis. Here, $\delta[\alpha_{\mathbf{k}}]$ is a 3×3 matrix in band space, with unity at the $(\alpha_{\mathbf{k}}, \alpha_{\mathbf{k}})$ element and zero elsewhere for state $\mathbf{k}$ on band $\alpha_{\mathbf{k}}$, and $u(\mathbf{k})$ is the unitary transformation that diagonalize the normal state Hamiltonian. Hence by taking the one-loop approximation to the electronic Green's function:

$$\mathcal{G}(\mathbf{k}, i\nu_m) = \mathcal{G}_0(\mathbf{k}, i\nu_m) + \mathcal{G}_0(\mathbf{k}, i\nu_m) \Sigma(\mathbf{k}, i\nu_m) \mathcal{G}_0(\mathbf{k}, i\nu_m), \tag{9}$$

where the $\mathcal{G}_0^{-1}(\mathbf{k}, i\nu_m) = \frac{1}{2}(i\nu_m - \tau^z h_{\mathbf{k}})$ is the bare electron Green's function (with $h_{\mathbf{k}}$ being the 3×3 tight-binding Hamiltonian of Eq. (2) in the orbital basis), the Dyson's equation of Eq. (5) can be readily reduced to the linearized gap equation of the form $\Delta(\mathbf{k}) = \sum_{\mathbf{k}'} V(\mathbf{k}, \mathbf{k}') \Delta(\mathbf{k}')$ whose eigenvalues represent the dimensionless effective BCS pairing interactions for the pairing channels satisfying Eq. (8); details are given in "Methods".

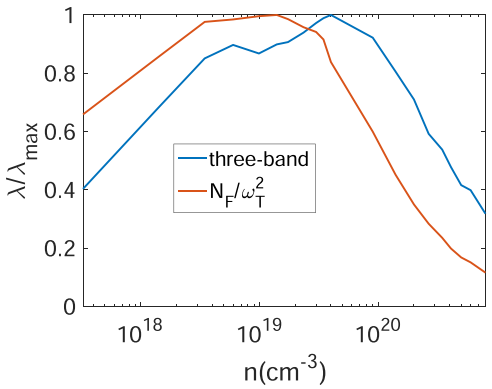

Fig. 2 BCS eigenvalue λ_{BCS}. Comparison between the BCS eigenvalue λ_{BCS} dome in the three-orbital model of Eq. (2) and the single-band model of Eq. (1). In the former, the weak tetragonal crystal field strength of ~2.2 meV[15] has been included, which has little effect around the optimal doping. For a better comparison on the superconducting dome, both lines are rescaled with respect to their maximal value. λ/λ_{max} is the rescaled BCS eigenvalue. Red line is the result from single-band estimation, while blue line is the result from three-band calculation.

The effective BCS interaction of the above three-band model derived from this procedure plotted in Fig. 2 with comparison with the single-band estimation of Eq. (1), demonstrates that the superconducting dome arises also with the unconventional, i.e. odd-parity, electron-phonon coupling of Eq. (4). While the optimal doping (and therefore chemical potential) value may be shifted, the suppression of superconductivity on the low density dome edge by the vanishing density of states and on the high density dome edge by the TO1 phonon hardening still remains. This remains qualitatively true as long as there is any non-zero screening effect on Eq. (4) that attenuates g at sufficiently high density (For $\langle \boldsymbol{\phi}_{\mathbf{q}=0} \rangle \neq 0$, Eq. (4) gives us the inversion symmetry breaking electron hopping, one of the key ingredients for the Rashba effect[44,53]. The reduction of the Rashba coefficient with the increasing carrier concentration found in the recent first-principle calculation for Bi_2WO_6, a related material[55], and the experiment on the few-layer GeTe[56] are possible instances of screening attenuating such electron hopping and by extension, the parameter g in Eq. (4), the simplest modeling of which is the density-independent gk_F we have used for obtaining Fig. 2.

Normal state considerations

We shall now show that the above phonon-mediated superconducting mechanism is consistent with T^2 resistivity that has been observed for $SrTiO_3$ at low doping[57]. This behavior has attracted attention because, given the small Fermi surface, it cannot be sufficiently explained by the electron-electron scattering process[58–60]. Our point here is that this behavior can be actually explained from the single-phonon electron-phonon scattering process, the imaginary part of the self-energy is given by the Fermi's golden rule (see Supplementary Information for

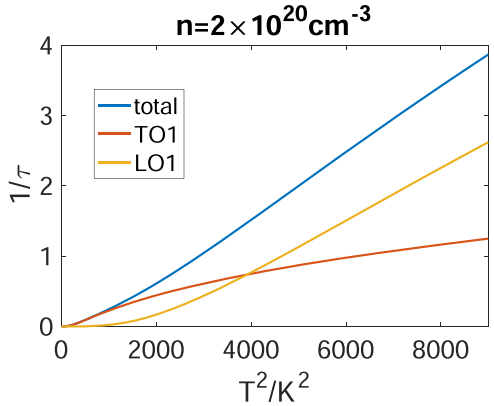

Fig. 3 T^2 scattering rate. (Blue) Scattering rate as a function of T^2. Contributions from TO1 (Red) and LO1 (yellow) phonons are included. Parameters $\omega_T = 6$ meV, $\omega_L = 20$ meV[6], $A_T = 1$ and $A_L = 15$ are taken. Blue line is the sum of the red (TO1 contribution) and yellow (LO1 contribution) line.

derivation):

$$\begin{aligned}\mathrm{Im}\Sigma(\mathbf{k},\epsilon) = -\pi\sum_{\mathbf{q}}|g_{\mathbf{k}',\mathbf{k}}|^2\big[\delta(\epsilon-\xi_{\mathbf{k}'}+\omega_{\mathbf{q}})(n_F(\xi_{\mathbf{k}'})+n_B(\omega_{\mathbf{q}}))\\ +\delta(\epsilon-\xi_{\mathbf{k}'}-\omega_{\mathbf{q}})(n_F(-\xi_{\mathbf{k}'})+n_B(\omega_{\mathbf{q}}))\big],\end{aligned} \tag{10}$$

where $\xi_{\mathbf{k}}$ and $\omega_{\mathbf{q}}$ are the dispersions of electrons and phonons. $g_{\mathbf{k}',\mathbf{k}}$ is the electron-phonon coupling strength (with $\mathbf{k}' = \mathbf{k}+\mathbf{q}$). n_F and n_B are the Fermi and Bose distributions. For the optical phonons, the Einstein model is sufficient to capture the qualitative behavior, i.e. $\omega_{\mathbf{q}} \approx \omega$. Therefore, if we focus on electrons at the Fermi surface, the self-energy from scattering off a single branch of optical phonons would be:

$$\mathrm{Im}\Sigma(\mathbf{k},\epsilon=0) = -2\pi[(n_F(\omega)+n_B(\omega))]\sum_{\mathbf{q}}|g_{\mathbf{k}',\mathbf{k}}|^2\delta(\xi_{\mathbf{k}'}-\omega), \tag{11}$$

from which the relation between the scattering rate and the self-energy $1/\tau = -2\mathrm{Im}\Sigma/\hbar$ gives us the scattering rate formula of the form:

$$1/\tau = A[(n_F(\omega)+n_B(\omega))]. \tag{12}$$

The simplified scattering rate depends on the phonon energy ω, temperature T and a coefficient A, proportional to the magnitude square of the electron-phonon coupling strength. By itself, Eq. (12) cannot give rise to the T^2 resistivity; the resistivity rather shows a T-linear behavior at high temperature $T \gg \omega$ and an exponential suppression at low temperature $T \ll \omega$ with a crossover regime for $T \sim \hbar\omega/k_B$.

The T^2 resistivity can nevertheless arise from scattering by multiple branches of optical phonons at different frequencies. As charge carrier density increases, the energy of the TO1 phonon increases from 20 K to 100 K in the T^2 resistivity measurement for Nb-doped STO[57]. Energies of other optical phonons are essentially doping-independent. Among them, the LO1 phonon has the lowest energy at ~200 K. Due to the strong electron-phonon coupling in the LO1 phonon channel[4], its contribution to the scattering rate should not be neglected. We thus have the combined electron-phonon scattering rate:

$$\begin{aligned}1/\tau = A_T[n_F(\omega_T,T)+n_B(\omega_T,T)]\\ +A_L[n_F(\omega_L,T)+n_B(\omega_L,T)]\end{aligned} \tag{13}$$

with $A_L \gg A_T$. This leads to a broad crossover regime starting from TO1 phonon energy, up to LO1 phonon energy. This crossover regime could give an approximate T^2 scattering rate, as shown in Fig. 3 for a doping at the superconducting dome. The temperature is much lower than the Fermi energy at this doping. At higher temperature, including electrons away from the Fermi surface may be needed for the computation of the scattering rate. Approximate T^2 resistivity at other dopant concentrations can be found in the Supplementary Information. To summarize, we note that while other mechanisms are possible[58], the measured phonon frequency values along with the calculations presented here make it impossible to rule out a scenario in which the coupling to both TO1 and LO1 phonon modes can produce the T^2 resistivity at least over a range of temperatures (Fig. 3).

DISCUSSION

In this paper, we have utilized experimental data to constrain and deduce the most likely pairing mechanism underlying Nb-doped $SrTiO_3$. Such strategies can perhaps be of broader relevance to other materials such as PbTe and $KTaO_3$ that are close to a ferroelectric transition. It would be of considerable interest to repeat such planar tunneling measurements in these systems. For example, the ideas presented here can help shed light on the recent observations of interfacial superconductivity in $KTaO_3$, which shows a surprisingly high T_c of ~2 K, while showing no signs of bulk superconductivity at the present time. At an interface, the presence of Rashba spin-orbit coupling allows for the coupling to a single TO1 phonon as in Eq. (4). The effective strength of the phonon coupling is enhanced by bulk spin-orbit coupling, which may account for the enhancement of superconductivity at the interface of this system. Further experimental studies in similar materials may help uncover the global phase diagram of quantum paraelectrics as a function of spin-orbit strength, dopant concentration, and spatial dimensionality.

METHODS

BCS eigenvalue calculation

The linearized gap equation:

$$\Delta(\mathbf{k}) = \sum_{\mathbf{k}'} V(\mathbf{k},\mathbf{k}')\Delta(\mathbf{k}'), \tag{14}$$

from the Dyson's equation of Eq. (5) need to have:

$$\begin{aligned}V(\mathbf{k},\mathbf{k}') = CN_F\sum_{ij}\chi_{ij,0}(\mathbf{k}'-\mathbf{k})\mathrm{Tr}\big\{M^\dagger(\mathbf{k})u^\dagger(\mathbf{k})F_j(\mathbf{k},\mathbf{k}'-\mathbf{k})\\ u(\mathbf{k}')M(\mathbf{k}')u^T(-\mathbf{k}')F_i(\mathbf{k},\mathbf{k}'-\mathbf{k})u^*(-\mathbf{k})\big\},\end{aligned} \tag{15}$$

where $M(\mathbf{k}) \equiv i\sigma^y\delta[a_{\mathbf{k}}]$, while the constant C is a function of energy cutoff and critical temperature, i.e.$C \propto \log(\omega_c/T_c)$. The eigenvalues of the linearized gap equation are exactly λ_{BCS}'s that determine T_c. Numerically, the above linearized gap equation can be treated as an eigenvalue equation of matrix $V(\mathbf{k},\mathbf{k}')$, in a vector space spanned by N momenta. T_c is determined by the largest eigenvalue, and the corresponding eigenvector (dominant pairing channel) is s-wave. The Fermi energy E_F, the carrier density n and the TO1 phonon energy ω_T are taken from the tunneling experiment[6]. We assume $N_F, k_F \propto \sqrt{E_F}$, and $c_T = 0$.

Scattering rate derivation

The formula for the scattering rate of electrons due to a single branch of phonons, as given in Eq. (12), can be derived from the one-loop electron self-energy. The generalized form of the electron-phonon coupling:

$$H_{\mathrm{e-ph}} = \sum_{\mathbf{q},\lambda}\sum_{\mathbf{k}} g_{\lambda;ss'}(\mathbf{q},\mathbf{k})(a_{\mathbf{q},\lambda}+a^\dagger_{-\mathbf{q},\lambda})c^\dagger_{\mathbf{k}+\mathbf{q},s}c_{\mathbf{k},s'}, \tag{16}$$

where $a(a^\dagger)$ is the phonon annihilation (creation) operator and λ the phonon polarization, can be taken as the starting point to obtain the one-loop electron self-energy:

$$\begin{aligned}\Sigma(\mathbf{k},i\omega_n) = \frac{k_BT}{\hbar}\frac{1}{\hbar}\sum_{\mathbf{q}}|g_\lambda(\mathbf{q},\mathbf{k})|^2\sum_{iv_m}\frac{1}{i\omega_n+iv_m-\xi_{\mathbf{k}+\mathbf{q}}}\frac{2\omega_{\mathbf{q},\lambda}}{v_m^2+\omega^2_{\lambda,\mathbf{q}}}\\ = \frac{1}{\hbar}\sum_{\mathbf{q}}|\tilde{g}_\lambda(\mathbf{q},\mathbf{k})|^2\left[\frac{n_B(\omega_{\lambda,\mathbf{q}},T)+n_F(\xi_{\mathbf{k}+\mathbf{q}},T)}{i\omega_n+\omega_{\lambda,\mathbf{q}}-\xi_{\mathbf{k}+\mathbf{q}}}+\frac{n_B(\omega_{\lambda,\mathbf{q}},T)+n_F(-\xi_{\mathbf{k}+\mathbf{q}},T)}{i\omega_n-\omega_{\lambda,\mathbf{q}}-\xi_{\mathbf{k}+\mathbf{q}}}\right],\end{aligned} \tag{17}$$

where $\omega_{\mathbf{q},\lambda}$ is the phonon eigenfrequency, in the Matsubara frequency. One can see how Eq. (10) can be obtained by taking the imaginary part of Eq. (17). Applying the Einstein model for phonons with $\omega_{\mathbf{q}} = \omega_0$ for all $\mathbf{q}$,

the scattering rate of Eq. (12) is obtained the imaginary part of the electron self-energy:

$$\frac{1}{\tau} = -\frac{2}{\hbar}\mathrm{Im}\Sigma(\omega + i\delta \to 0), \tag{18}$$

with:

$$A = \frac{2\pi}{\hbar^2}\sum_{\mathbf{k}'}|\tilde{g}(\mathbf{k}' - \mathbf{k}, \mathbf{k})|^2[\delta(\xi_{\mathbf{k}'}/\hbar - \omega_0) + \delta(\xi_{\mathbf{k}'}/\hbar + \omega_0)]. \tag{19}$$

Note added to proof

While drafting this manuscript, we have learnt of the recent preprint by Gastiasoro et al.[40] which which has some overlap with the ideas presented here. However, our motivation here is distinct in the use of recent tunneling experiments to constrain pairing mechanisms.

DATA AVAILABILITY

Relevant data in this paper are available upon reasonable request.

Received: 8 November 2021; Accepted: 14 May 2022;
Published online: 14 June 2022

REFERENCES

1. Schooley, J. F., Hosler, W. R. & Cohen, M. L. Superconductivity in semiconducting $SrTiO_3$. *Phys. Rev. Lett.* **12**, 474–475 (1964).
2. Koonce, C. S., Cohen, M. L., Schooley, J. F., Hosler, W. R. & Pfeiffer, E. R. Superconducting transition temperatures of semiconducting $SrTiO_3$. *Phys. Rev.* **163**, 380–390 (1967).
3. Lin, X. et al. Critical doping for the onset of a two-band superconducting ground state in $SrTiO_{3-\delta}$. *Phys. Rev. Lett.* **112**, 207002 (2014).
4. Swartz, A. G. et al. Polaronic behavior in a weak-coupling superconductor. *Proc. Natl Acad. Sci. USA* **115**, 1475–1480 (2018).
5. Thiemann, M. et al. Single-gap superconductivity and dome of superfluid density in Nb-doped $SrTiO_3$. *Phys. Rev. Lett.* **120**, 237002 (2018).
6. Yoon, H. et al. Low-density superconductivity in $SrTiO_3$ bounded by the adiabatic criterion. Preprint at https://doi.org/10.48550/arXiv.2106.10802 (2021).
7. Ueno, K. et al. Discovery of superconductivity in $KTaO_3$ by electrostatic carrier doping. *Nat. Nanotechnol.* **6**, 408–412 (2011).
8. Chen, Z. et al. Two-dimensional superconductivity at the $LaAlO_3/KTaO_3$(110) heterointerface. *Phys. Rev. Lett.* **126**, 026802 (2021).
9. Liu, C. et al. Two-dimensional superconductivity and anisotropic transport at $KTaO_3$ (111) interfaces. *Science* **371**, 716–721 (2021).
10. Chen, Z. et al. Electric field control of superconductivity at the $LaAlO_3/KTaO_3$(111) interface. *Science* **372**, 721–724 (2021).
11. Matsushita, Y., Wianecki, P. A., Sommer, A. T., Geballe, T. H. & Fisher, I. R. Type II superconducting parameters of Tl-doped PbTe determined from heat capacity and electronic transport measurements. *Phys. Rev. B* **74**, 134512 (2006).
12. Anderson, P. W. & Blount, E. I. Symmetry considerations on martensitic transformations: "ferroelectric" metals? *Phys. Rev. Lett.* **14**, 217–219 (1965).
13. Enderlein, C. et al. Superconductivity mediated by polar modes in ferroelectric metals. *Nat. Commun.* **11**, 4852 (2020).
14. van der Marel, D., Barantani, F. & Rischau, C. W. Possible mechanism for superconductivity in doped $SrTiO_3$. *Phys. Rev. Res.* **1**, 013003 (2019).
15. Gastiasoro, M. N., Ruhman, J. & Fernandes, R. M. Superconductivity in dilute SrTiO3: A review. *Ann. Phys.* **417**, 168107 (2020).
16. Volkov, P. A., Chandra, P. & Coleman, P. Superconductivity from energy fluctuations in dilute quantum critical polar metals. Preprint at https://doi.org/10.48550/arXiv.2106.11295 (2021).
17. Migdal, A. Interaction between electrons and lattice vibrations in a normal metal. *Sov. Phys. JETP* **7**, 996–1001 (1958).
18. Eliashberg, G. Interactions between electrons and lattice vibrations in a superconductor. *Sov. Phys. JETP* **11**, 696–702 (1960).
19. Pietronero, L., Strässler, S. & Grimaldi, C. Nonadiabatic superconductivity. I. vertex corrections for the electron-phonon interactions. *Phys. Rev. B* **52**, 10516–10529 (1995).
20. Grimaldi, C., Pietronero, L. & Strässler, S. Nonadiabatic superconductivity. II. Generalized Eliashberg equations beyond Migdal's theorem. *Phys. Rev. B* **52**, 10530–10546 (1995).
21. Chubukov, A. V., Abanov, A., Esterlis, I. & Kivelson, S. A. Eliashberg theory of phonon-mediated superconductivity-when it is valid and how it breaks down. *Ann. Phys.* **417**, 168190 (2020).
22. Reyren, N. et al. Superconducting interfaces between insulating oxides. *Science* **317**, 1196–1199 (2007).
23. Valentinis, D. et al. Modulation of the superconducting critical temperature due to quantum confinement at the $LaAlO_3/SrTiO_3$ interface. *Phys. Rev. B* **96**, 094518 (2017).
24. Gurevich, L. V., Larkin, A. I. & Firsov, Y. A. Possibility of superconductivity in semiconductors. *Sov. Phys. Sol. State* **4**, 131–135 (1962).
25. Kedem, Y. Novel pairing mechanism for superconductivity at a vanishing level of doping driven by critical ferroelectric modes. *Phys. Rev. B* **98**, 220505 (2018).
26. Kozii, V., Bi, Z. & Ruhman, J. Superconductivity near a ferroelectric quantum critical point in ultralow-density Dirac materials. *Phys. Rev. X* **9**, 031046 (2019).
27. Gastiasoro, M. N., Trevisan, T. V. & Fernandes, R. M. Anisotropic superconductivity mediated by ferroelectric fluctuations in cubic systems with spin-orbit coupling. *Phys. Rev. B* **101**, 174501 (2020).
28. Appel, J. Soft-Mode superconductivity in $SrTiO_{3-x}$. *Phys. Rev.* **180**, 508–516 (1969).
29. Takada, Y. Theory of superconductivity in polar semiconductors and its application to n-type semiconducting $SrTiO_3$. *J. Phys. Soc. Jpn.* **49**, 1267–1275 (1980).
30. Edge, J. M., Kedem, Y., Aschauer, U., Spaldin, N. A. & Balatsky, A. V. Quantum critical origin of the superconducting dome in $SrTiO_3$. *Phys. Rev. Lett.* **115**, 247002 (2015).
31. Gor'kov, L. P. Phonon mechanism in the most dilute superconductor n-type $SrTiO_3$. *Proc. Natl Acad. Sci. USA* **113**, 4646–4651 (2016).
32. Ruhman, J. & Lee, P. A. Superconductivity at very low density: the case of strontium titanate. *Phys. Rev. B* **94**, 224515 (2016).
33. Wölfle, P. & Balatsky, A. V. Superconductivity at low density near a ferroelectric quantum critical point: doped $SrTiO_3$. *Phys. Rev. B* **98**, 104505 (2018).
34. Gastiasoro, M. N., Chubukov, A. V. & Fernandes, R. M. Phonon-mediated superconductivity in low carrier-density systems. *Phys. Rev. B* **99**, 094524 (2019).
35. Klimin, S. et al. Superconductivity in $SrTiO_3$: dielectric function method for non-parabolic bands. *J. Supercond. Nov. Magn.* **32**, 2739–2744 (2019).
36. Bäuerle, D., Wagner, D., Wöhlecke, M., Dorner, B. & Kraxenberger, H. Soft modes in semiconducting $SrTiO_3$: II. The ferroelectric mode. *Z. Phys. B Condens. Matter* **38**, 335–339 (1980).
37. van Mechelen, J. L. M. et al. Electron-Phonon Interaction and charge carrier mass enhancement in $SrTiO_3$. *Phys. Rev. Lett.* **100**, 226403 (2008).
38. Choudhury, N., Walter, E. J., Kolesnikov, A. I. & Loong, C.-K. Large phonon band gap in $SrTiO_3$ and the vibrational signatures of ferroelectricity in $ATiO_3$ perovskites: first-principles lattice dynamics and inelastic neutron scattering. *Phys. Rev. B* **77**, 134111 (2008).
39. Ngai, K. L. Two-phonon deformation potential and superconductivity in degenerate semiconductors. *Phys. Rev. Lett.* **32**, 215–218 (1974).
40. Gastiasoro, M. N., Eleonora Temperini, M., Barone, P. & Lorenzana, J. Theory of Rashba coupling mediated superconductivity in incipient ferroelectrics. Preprint at https://doi.org/10.48550/arXiv.2109.13207 (2021).
41. Bistritzer, R., Khalsa, G. & MacDonald, A. H. Electronic structure of doped d^0 perovskite semiconductors. *Phys. Rev. B* **83**, 115114 (2011).
42. van der Marel, D., van Mechelen, J. L. M. & Mazin, I. I. Common Fermi-liquid origin of T^2 resistivity and superconductivity in n-type $SrTiO_3$. *Phys. Rev. B* **84**, 205111 (2011).
43. Zhong, Z., Tóth, A. & Held, K. Theory of spin-orbit coupling at $LaAlO_3/SrTiO_3$ interfaces and $SrTiO_3$ surfaces. *Phys. Rev. B* **87**, 161102 (2013).
44. Park, S. R., Kim, C. H., Yu, J., Han, J. H. & Kim, C. Orbital-angular-momentum based origin of Rashba-type surface band splitting. *Phys. Rev. Lett.* **107**, 156803 (2011).
45. Volkov, P. A. & Chandra, P. Multiband quantum criticality of polar metals. *Phys. Rev. Lett.* **124**, 237601 (2020).
46. Brydon, P. M. R., Das Sarma, S., Hui, H.-Y. & Sau, J. D. Odd-parity superconductivity from phonon-mediated pairing: application to $Cu_xBi_2Se_3$. *Phys. Rev. B* **90**, 184512 (2014).
47. Scheurer, M. S. Mechanism, time-reversal symmetry, and topology of superconductivity in noncentrosymmetric systems. *Phys. Rev. B* **93**, 174509 (2016).
48. Lee, M., Lee, H.-J., Lee, J. H. & Chung, S. B. Topological superconductivity from transverse optical phonons in oxide heterostructures. *Phys. Rev. Mater.* **4**, 034202 (2020).
49. Kim, H. et al. Beyond triplet: unconventional superconductivity in a spin-3/2 topological semimetal. *Sci. Adv.* **4**, eaao4513 (2018).
50. Venderbos, J. W. F., Savary, L., Ruhman, J., Lee, P. A. & Fu, L. Pairing states of spin-$\frac{3}{2}$ fermions: symmetry-enforced topological gap functions. *Phys. Rev. X* **8**, 011029 (2018).
51. Kozii, V. & Fu, L. Odd-parity superconductivity in the vicinity of inversion symmetry breaking in spin-orbit-coupled systems. *Phys. Rev. Lett.* **115**, 207002 (2015).
52. Wang, Y., Cho, G. Y., Hughes, T. L. & Fradkin, E. Topological superconducting phases from inversion symmetry breaking order in spin-orbit-coupled systems. *Phys. Rev. B* **93**, 134512 (2016).

53. Kim, M., Ihm, J. & Chung, S. B. Strongly enhanced Rashba splittings in an oxide heterostructure: a tantalate monolayer on $BaHfO_3$. *Phys. Rev. B* **94**, 115431 (2016).
54. Frigeri, P. A., Agterberg, D. F., Koga, A. & Sigrist, M. Superconductivity without inversion symmetry: MnSi versus $CePt_3Si$. *Phys. Rev. Lett.* **92**, 097001 (2004).
55. Djani, H. et al. Rationalizing and engineering rashba spin-splitting in ferroelectric oxides. *npj Quantum Mater.* **4**, 51 (2019).
56. Yang, X. et al. Three-dimensional limit of bulk Rashba effect in ferroelectric semiconductor GeTe. *Nano Lett.* **21**, 77–83 (2021).
57. Lin, X., Fauqué, B. & Behnia, K. Scalable T^2 resistivity in a small single-component Fermi surface. *Science* **349**, 945–948 (2015).
58. Kumar, A., Yudson, V. I. & Maslov, D. L. Quasiparticle and nonquasiparticle transport in doped quantum paraelectrics. *Phys. Rev. Lett.* **126**, 076601 (2021).
59. Verma, A., Kajdos, A. P., Cain, T. A., Stemmer, S. & Jena, D. Intrinsic mobility limiting mechanisms in lanthanum-doped strontium titanate. *Phys. Rev. Lett.* **112**, 216601 (2014).
60. Zhou, J.-J., Hellman, O. & Bernardi, M. Electron-phonon scattering in the presence of soft modes and electron mobility in $SrTiO_3$ perovskite from first principles. *Phys. Rev. Lett.* **121**, 226603 (2018).

ACKNOWLEDGEMENTS

We thank Piers Coleman, Rafael Fernandes, Changyoung Kim, Dmitrii Maslov, and Hyeok Yoon for useful discussions. Y.Y., H.Y.H., and S.R. were supported by the Department of Energy, Office of Basic Energy Sciences, Division of Materials Sciences and Engineering, under contract No. DEAC02-76SF00515. S.B.C. was supported by the National Research Foundation of Korea (NRF) grants funded by the Korea government (MSIT) (2020R1A2C1007554) and the Ministry of Education (2018R1A6A1A06024977).

AUTHOR CONTRIBUTIONS

Y.Y. performed numerical calculation. All authors contributed to designing the project and writing the manuscript.

COMPETING INTERESTS

The authors declare no competing interests.

ADDITIONAL INFORMATION

Supplementary information The online version contains supplementary material available at https://doi.org/10.1038/s41535-022-00466-2.

Correspondence and requests for materials should be addressed to S. Raghu or Suk Bum Chung.

Reprints and permission information is available at http://www.nature.com/reprints

Publisher's note Springer Nature remains neutral with regard to jurisdictional claims in published maps and institutional affiliations.